ONCOIMMUNOLOGY
2023, VOL. 12, NO. 1, 2259212
https://doi.org/10.1080/2162402X.2023.2259212

Taylor & Francis
Taylor & Francis Group

ORIGINAL RESEARCH

OPEN ACCESS Check for updates

PB101, a VEGF- and PlGF-targeting decoy protein, enhances antitumor immunity and suppresses tumor progression and metastasis

Eun-Jin Go[a,b*], Hannah Yang[a,b*], Seung Joon Lee[a,b*], Hyun Gul Yang[c], Jin A. Shin[c], Won Suk Lee[a,b], Hye Seong Lim[c], Hong Jae Chon[a,b], and Chan Kim[a,b]

[a]Medical Oncology, CHA Bundang Medical Center, CHA University School of Medicine, Seongnam, Gyeonggi-do, Republic of Korea; [b]Laboratory of Translational Immuno-Oncology, CHA University School of Medicine, Seongnam, Gyeonggi-do, Republic of Korea; [c]Panolos Bioscience, Inc, Hwaseong-si, Republic of Korea

ABSTRACT

Antiangiogenic therapy is a recognized method for countering the immunosuppressive tumor microenvironment (TME) and improving anti-tumor immunity. PB101 is a glycosylated decoy receptor that binds to VEGF-A and PlGF with high affinity, based on the VEGFR1 backbone. Here, we elucidated PB101-induced remodeling of tumor angiogenesis and immunity, which enhances anti-PD-L1 immune checkpoint blockade. PB101 inhibited tumor growth by suppressing angiogenesis and enhancing $CD8^+$ T cell infiltration into the tumors. PB101 induced robust reprogramming of antitumor immunity and activates intratumoral $CD8^+$ T cells. Anti-tumor efficacy of PB101 is mostly dependent on $CD8^+$ T cells and IFN-γ. PB101 reprograms tumor immunity in a manner distinct from that of the conventional VEGF decoy receptor, VEGF-trap. With its potent immune-modulating capability, PB101 synergizes with an anti-PD-L1, triggering strengthened antitumor immunity. Combining PB101 and anti-PD-L1 could establish durable protective immunity against tumor recurrence and metastasis. The findings of this study offer scientific rationales for further clinical development of PB101, particularly when used in combination with immune checkpoint inhibitors, as a potential treatment for advanced cancers.

ARTICLE HISTORY
Received 11 May 2023
Revised 8 September 2023
Accepted 11 September 2023

KEYWORDS
Angiogenesis; combination immunotherapy; immune checkpoint inhibitor; PB101; PlGF; tumor immunity; VEGF-A

Introduction

Tumor angiogenesis is an essential mechanism for tumor growth, progression, and metastasis of cancer, and is driven by diverse proangiogenic factors, with vascular endothelial growth factor (VEGF) being the most important.[1–5] Over the last two decades, various antibodies, small-molecule inhibitors, and recombinant proteins targeting the VEGF family and its receptors have been developed that are now used as standard treatments for several malignancies.[1,2,4] However, monotherapy with antiangiogenic agents is often cytostatic and only provides transient and modest survival benefits.[2,5,6] Moreover, some preclinical studies have raised concerns that excessive suppression of angiogenesis may accelerate tumor invasion and metastasis depending on the tumor stage and the duration of antiangiogenic treatment.[7,8]

Although VEGF was initially discovered as an angiogenic factor, it is now increasingly recognized as an immunosuppressive factor that regulates both innate and adaptive immunity within the TME.[9–11] Consequently, VEGF/VEGFR-targeting therapies have attracted attention as they have been found to enhance anti-cancer immune responses within the TME.[2–4] During the last 5 years, combination therapies of angiogenesis inhibitors and immune checkpoint inhibitors have been shown to induce the most potent and durable anticancer immune responses in preclinical and clinical studies, and have become the new gold standard for the treatment of liver, kidney, lung, and endometrial cancers.[3,12–16] Therefore, when developing angiogenesis inhibitors, both antiangiogenic and immune reprogramming mechanisms should be evaluated to achieve optimal therapeutic efficacy.

Placental growth factor (PlGF) is a pro-angiogenic factor that was first discovered in the placenta and belongs to the VEGF family of ligands.[17] PlGF binds to VEGFR1 on endothelial cells to regulate endothelial cell sprouting, mitogenesis, cell migration, and vascular permeability, and regulates immune responses by engaging VEGFR1 in hematopoietic cells.[18–21] In the TME, PlGF is known to play protumoral immunosuppressive roles by inhibiting the maturation and antigen presentation of dendritic cells and regulating the survival and polarization of tumor-associated macrophages (TAMs).[18,22,23] Furthermore, it inhibits cytotoxicity and cytokine production in intratumoral NK cells.[18,22] Moreover, activated T cells not only express VEGFR2 but also VEGFR1, and the engagement of VEGFR[24,25] in these cells can directly modulate T cell functions, such as T cell trafficking or IL-10 production.[18,26]

Previously, we developed PB101, a glycosylated soluble decoy receptor fusion protein for VEGF and PlGF, by fusing the immunoglobulin homology (Ig)-like domains 2 and 3 of

CONTACT Chan Kim chan@cha.ac.kr; Hong Jae Chon minidoctor@cha.ac.kr Medical Oncology, CHA Bundang Medical Center, CHA University School of Medicine, 59 Yatap-ro, Bundang-gu, Seongnam 13496, Republic of Korea
*These authors equally contributed to this work.
Supplemental data for this article can be accessed online at https://doi.org/10.1080/2162402X.2023.2259212

VEGFR1 to IgG1-Fc.[27–29] PB101 exhibited enhanced decoy activity against VEGF-A and PlGF, compared with VEGF-trap.[27,28] This advantage was attributed to the VEGFR1 backbone of PB101, which enabled its robust antiangiogenic, antitumor, and antimetastatic efficacies in various tumor models.[27,29] However, the mechanisms of action other than antiangiogenesis, especially immune modulation, have not yet been elucidated.

In this study, we reveal how PB101 reprograms tumor immunity and overcomes aberrant angiogenesis within the TME in a manner that is distinct from that of the conventional VEGF decoy receptor, VEGF-trap. With its potent immune-modulating capability, PB101 synergizes with an anti-PD-L1 checkpoint inhibitor and triggers strengthened antitumor immunity and durable cancer control.

Materials and methods

Mice and cell line

C57BL/6 mice (7 weeks old, male) were purchased from JA Bio (Suwon, Korea) and maintained in a specific pathogen-free animal facility at CHA University (Seongnam, Korea). The MC38 colon cancer cell line was purchased from National Cancer Center (Goyang, South Korea). To generate a VEGF-overexpressing liver cancer cell line (Hepa-V liver cancer), Hepa 1–6 cells were transfected with a lentivirus encoding VEGF-A (NM_001287057.1, Ex-Mm06015-Lv219, GeneCopoeia). Transfected cells were selected via culturing in media containing 2 μg/mL puromycin for 7 days and validated for VEGF-A expression. MC38 and Hepa-V liver cancer cells were cultured in Dulbecco's modified Eagle medium supplemented with 10% fetal bovine serum and 1% penicillin/streptomycin at 37°C with 5% CO_2.

Tumor models and treatment regimens

To confirm the efficacy of PB101, MC38 colon cancer cells (2×10^5 cells/mouse), or Hepa-V liver cancer cells (5×10^5 cells/mouse) were injected into the right flank of C57BL/6 mice. When the tumor volumes exceeded 50 mm^3, mice were intraperitoneally injected with PB101 (25 mg/kg), phosphate-buffered saline (PBS), anti-CD8 (200 μg, clone 53–6.7, BioXCell), anti-CD4 (200 μg, clone GK1.5, BioXCell), anti-interferon (IFN)-γ (200 μg, clone XMG1.2, BioXCell), VEGF-trap (25 mg/kg), anti-LAG-3 (200 μg, clone C9B7W, BioXCell) or anti-PD-L1 (200 μg, clone 10F.9G2, BioXCell) at indicated time points. PB101 and VEGF-trap were provided by Panolos Bioscience, Inc., Korea. For rechallenge experiments, Hepa-V liver cancer cells were injected subcutaneously into the right flank (2×10^6 cells) and intravenously into tail vein (1×10^6 cells) of C57BL/6 mice with complete tumor regression or untreated naïve mice.

Flow cytometry analysis

For flow cytometry analysis, the harvested tumor tissues were dissociated into single cells. Each group was minced and incubated for 1 h at 37°C in a digestion buffer comprising 40 μg/ml DNase 1 (Roche) and 2 mg/ml Collagenase D (Roche). Prior to antibody staining, cell suspensions were filtered through a 70-μm cell strainer (Corning). Subsequently, the cells were incubated on ice for 30 min in the Fixable Viability Dye eFluor 450 (Invitrogen) to remove dead cells. Cells were then incubated with FACS buffer containing the following primary antibodies: anti-CD45 (clone 30-F11, BD Biosciences), anti-CD3 (clone 145-2c11, eBioscience), anti-CD8 (clone 53–6.7, eBioscience), anti-CD4 (clone RM4–5, eBioscience), anti-CD11c (clone N418, eBioscience), anti-CD11b (clone M1/70, eBioscience), and anti-F4/80 (clone BM8, eBioscience). The cells were further permeabilized using the Foxp3/Transcription Factor Staining Buffer Set (eBioscience) and stained for Foxp3 (clone FJK-16s, eBioscience), GzB (clone QA16A02, BioLegend), Nos2 (clone CXNFT, eBioscience), and Arg1 (clone A1exF5, eBioscience). Flow cytometry was performed using a CytoFLEX flow cytometer (Beckman Coulter), and the data were analyzed using FlowJo software version 10 (Tree Star Inc.).

Histological analyses

For immunofluorescence staining, tumor tissues were fixed in 1% paraformaldehyde, dehydrated in 20% sucrose overnight, and embedded in a tissue-freezing medium (Leica). The frozen samples were sectioned into 20-μm-thick slices. The samples were incubated overnight with the following primary antibodies: anti-CD8 (rat, clone 53–6.7, BD Bioscience), anti-CD31 (rabbit polyclonal, Abcam), anti-Granzyme B (GzB, rat, clone NGZB, Invitrogen), anti-CD206 (rat, clone MR5D3, Invitrogen), anti-Nos2 (rabbit polyclonal, Abcam), anti-caspase 3 (rabbit polyclonal, R&D System), Next, the samples were incubated for 2 h at room temperature with the following secondary antibodies: FITC-conjugated anti-rat IgG (Jackson ImmunoResearch), Cy3-conjugated anti-rat IgG (Jackson ImmunoResearch), Cy3-conjugated anti-rabbit IgG (Jackson ImmunoResearch), FITC-conjugated anti-rabbit IgG (Jackson ImmunoResearch). Cell nuclei were counterstained with 4′6-diamidino-2-phenylindole (Invitrogen), and samples were mounted using fluorescent mounting medium (DAKO, Denmark). Images were acquired using an LSM 880 microscope (Carl Zeiss). The densities of blood vessels, T lymphocytes, GzB^+ cell area, M1-like macrophages, M2-like macrophages and caspase 3^+ apoptosis cells were calculated using ImageJ software (http://rsb.info.nih.gov/ij). Blood vessel density was determined by calculating the $CD31^+$ area per 0.49 mm^2 of the tumor sections. The degree of cytotoxic T lymphocyte infiltration was calculated as the percentage of $CD8^+$ area per random 0.49 mm^2 field. To define the activation of T lymphocytes, the GzB^+ area per 0.49 mm^2 was calculated in intratumoral regions. The degree of infiltration of M1- or M2-like macrophages was determined as the percentage of $NOS2^+$ or $CD206^+$ area per 0.49 mm^2, respectively. All analyses were performed in at least five 0.49 mm^2 fields per mouse.

For hematoxylin and eosin (H&E) staining, the lung tissues were fixed overnight in 4% paraformaldehyde and embedded in paraffin. The samples were sectioned into 5-μm-thick slices and stained with H&E.

NanoString gene expression analysis

The mice were treated with PB101 (25 mg/kg) five times every 2 or 3 d, and tumor tissues were harvested for NanoString analysis 24 h after the last treatment. The NanoString analysis was performed on four tumor samples in each group. Immune profiling was performed with a digital multiplexed NanoString nCounter PanCancer Immune Profiling mouse panel (NanoString Technologies) using 100 ng of total RNA isolated from tumor samples as previously described.[30,31] Data analysis was performed using nSolver software (NanoString Technologies), as previously described. The mRNA profiling data were normalized against the housekeeping gene and analyses were performed using R software (www.rproject.org).

Statistical analysis

All statistical analyses were performed using GraphPad Prism software (version 7.0; La Jolla, CA, USA) and PASW Statistics 18 (SPSS, Chicago, IL, USA). Values are presented as mean ± SD unless otherwise indicated. Statistical significance was set at $P < .05$.

Results

PB101 suppresses tumor angiogenesis and enhances intratumoral CD8$^+$ T cell infiltration

To confirm the antitumor efficacy of PB101, MC38-bearing mice were treated with PBS or PB101. After five consecutive treatments, PB101 (25 mg/kg) suppressed MC38 tumor growth by 66.2% compared to the PBS-treated control group (Figure 1a,b). Histological analysis revealed that PB101 suppressed CD31$^+$ tumor blood vessels by 57.7%, enhanced CD8$^+$ T cell infiltration by 2.5-fold, and caspase 3$^+$ apoptotic cells by 2.1-fold compared to PBS-treated controls (Figure 1c,d).

PB101 reprograms antitumor immunity

Flow cytometry and histological analyses were performed to investigate how PB101 regulates innate and adaptive immunity within the TME. PB101 increased the proportion of tumor-infiltrating CD11c$^+$ dendritic cells (Figure 2a) while decreasing the infiltration of CD11b$^+$F4/80$^+$tumor-associated macrophages (TAMs) (Figure 2b) compared with PBS-treated control tumors. Furthermore, PB101 increased the proportion of M1-like macrophages and decreased the proportion of M2-like macrophages, thus increasing the M1/M2 ratio (Figure 2c). Histological analysis showed consistent findings: an increase in NOS2$^+$ M1-like macrophages and a decrease in CD206$^+$ M2-like macrophages (Figure 2d). Furthermore, PB101 enhanced the infiltration of CD3$^+$ (Figure 2e) and CD8$^+$ T cells (Figure 2f). Histological analysis revealed an increase in the number of GzB$^+$-activated CD8$^+$ T cells within the TME after PB101 treatment (Figure 2g). Taken together, these results suggest that PB101 induces robust antitumor responses by enhancing innate/adaptive immunity in the TME.

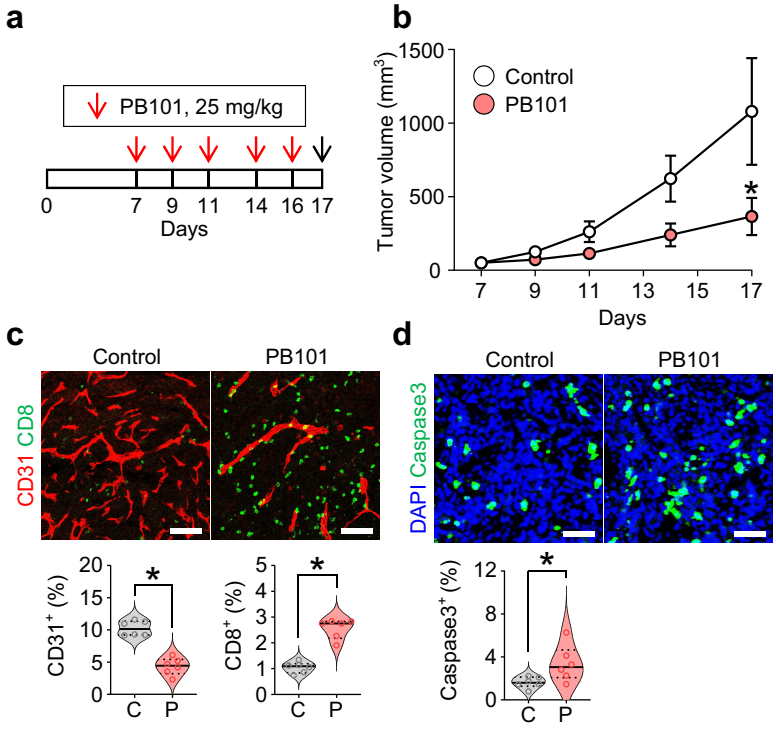

Figure 1. PB101 suppresses tumor angiogenesis and enhances intratumoral CD8$^+$ T cell infiltration. a. Diagram depicting treatment schedule in MC38 colon cancer. Red and black arrows indicate treatment and sacrifice, respectively. b. Comparison of tumor growth in mice treated with phosphate-buffered saline (PBS) or PB101. Pooled data from three independent experiments with N = 10 per group. c. Representative images and quantifications of CD31$^+$ blood vessels and CD8$^+$ T cells within tumors. d. Representative images and quantifications of caspase 3$^+$ apoptosis cells within tumors. N = 6 per group. Scale bars, 100 µm. Values are shown as the mean ± SD. *$P < .05$ vs control.

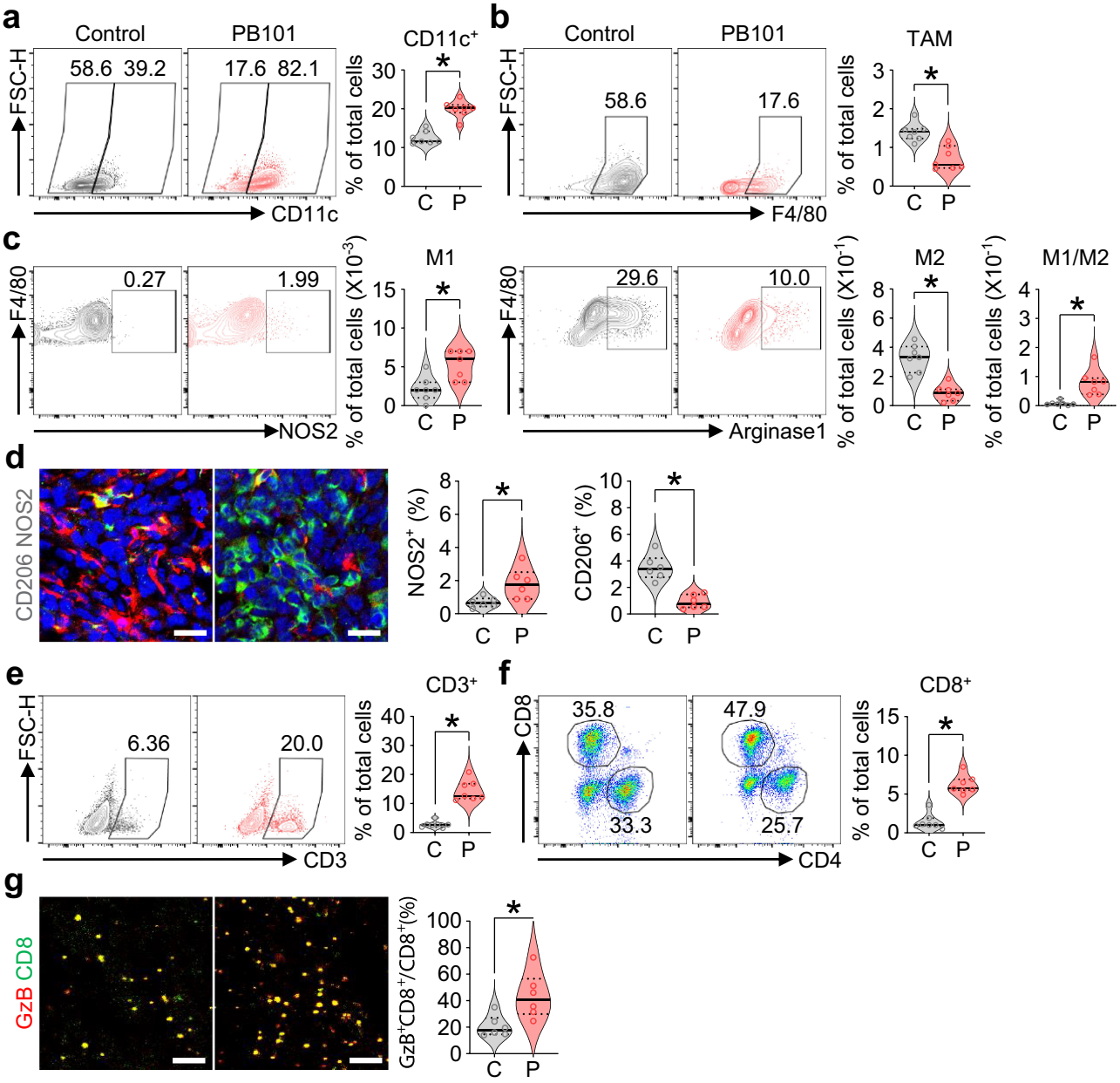

Figure 2. PB101 reprograms antitumor immunity. a – c. Representative flow cytometric plot and comparisons of $CD11c^+$ dendritic cells (a), $CD11b^+F4/80^+$ tumor-associated macrophages (TAMs), and of $NOS2^+$ M1-like and Arginase 1^+ M2-like TAMs (c) within tumors. d. Representative images and quantification of $NOS2^+$ M1-like macrophages and $CD206^+$ M2-like macrophages within the tumors. Scale bars, 20 μm. E and F. Representative flow cytometric plot and comparison of tumor-infiltrating $CD3^+$ T cells (e) and $CD8^+$ T cells (f). G. Representative images and quantification of granzyme B (GzB)-expressing $CD8^+$ T cells. Scale bars, 100 μm. N = 6–7 per group. Values are shown as the mean ± SD. *$P < .05$ vs control.

PB101 depends on $CD8^+$ T cells and IFN-γ to suppress tumor growth

To comprehensively analyze the PB101-induced immune reprogramming in the TME, we analyzed immune-related gene signatures using NanoString PanCancer Immune Profiling (Figure 3). PB101 broadly reprogrammed immune-related genes, and enhanced genes related to $CD8^+$ T cells, such as *Cd8a*, *Gzma*, and *Ifn-γ* (Figure 3a–b). Gene Ontology enrichment analysis also showed strong enrichment of gene sets involved in lymphocyte activation and differentiation (Figure 3c). In particular, PB101 considerably upregulated genes related to lymphocyte-endothelial cell interactions, which are critical for lymphocyte trafficking to the TME.[32] Dendritic cell markers were also enhanced in PB101-treated tumors compared to control tumors. Moreover, PB101 treatment elicited strong IFN, Th1, and Th2 responses and T cell activation within the tumors (Figure 3d).

To define the immune components responsible for antitumor efficacy of PB101, MC38 tumor-bearing mice were treated with PB101 in combination with various neutralizing antibodies (αCD4, αCD8, and αIFN-γ) (Figure 3e–f and Supplementary Figure S1). Although depletion of $CD4^+$ T cells did not affect tumor growth suppression by PB101, depletion of $CD8^+$ T cells or IFN-γ markedly abrogated antitumor efficacy of PB101 (Figure 3f).

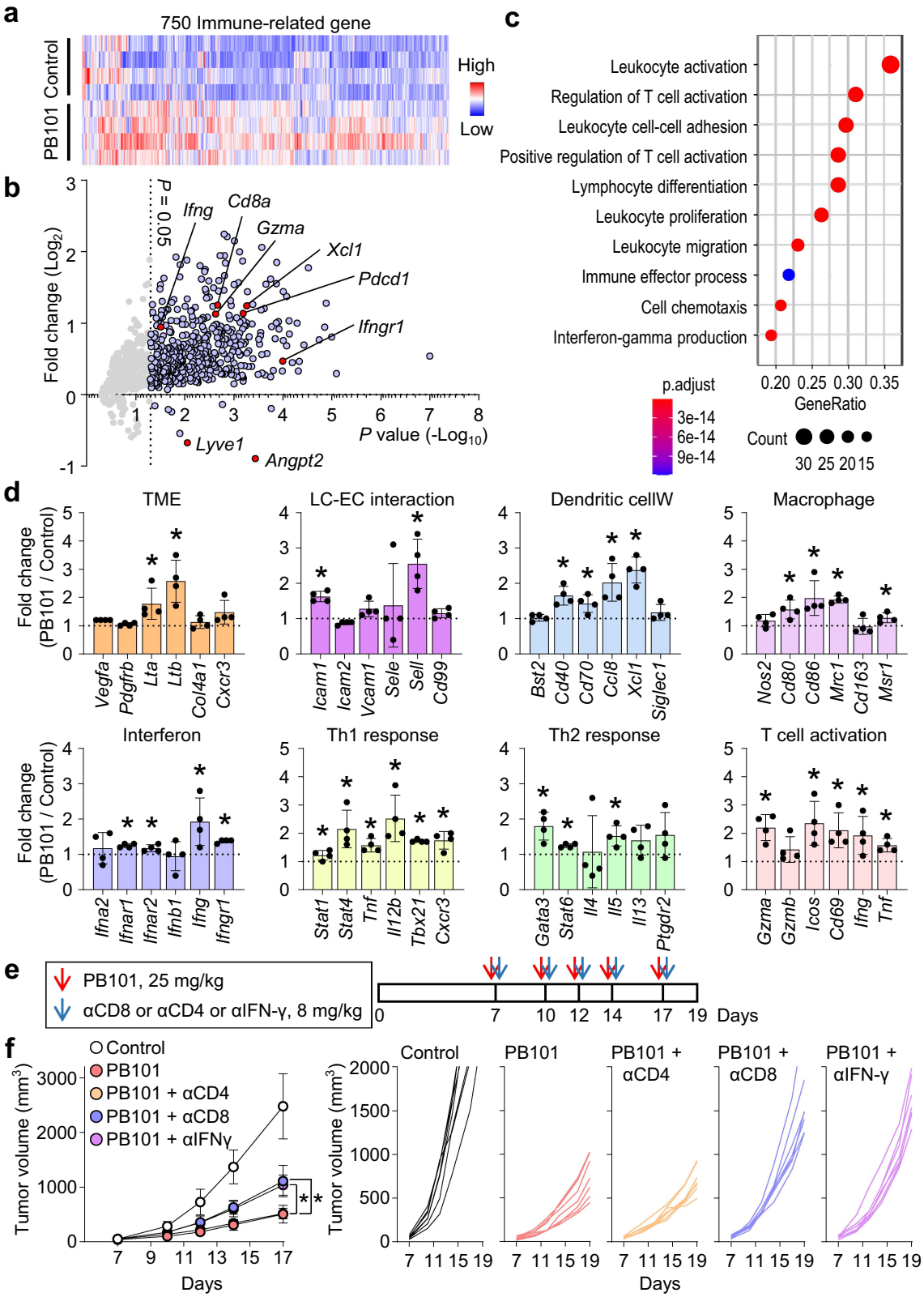

Figure 3. PB101 depends on CD8$^+$ T cells and interferon (IFN)-γ to suppress tumor growth. a. Heatmap of NanoString immune-related gene expression in PB101-treated or PBS-treated control tumors. N = 4 per group. b. Volcano plot showing the changes of gene expression in PB101-treated tumors compared to control tumors. c. Dot plot showing enrichment of gene ontology (GO) biological processes for immune-related genes in tumors treated with PB101. The size of each dot represents the number of genes significantly associated with a GO term, and the color of the dots represent the P-adjusted value. d. Comparisons of gene expression related to the tumor microenvironment (TME), lymphocyte (LC)-endothelial cell (EC) interaction, dendritic cell, macrophage, IFN, Th1/Th2 responses, and T cell activation. *$P < .05$ vs. control. e. Diagram depicting the treatment schedule of the PB101, anti-CD4, anti-CD8 and anti-IFN-γ. f. Comparison of individual tumor growth over time. N = 7 per group. *$P < .05$ vs PB101.

Therefore, PB101 mainly acted through $CD8^+$ T cells and IFN-γ-mediated immunity as well as its antiangiogenic effect.

PB101 shows distinct immunologic mechanisms of action compared to VEGF blockade

VEGF-trap (aflibercept) is a chimeric decoy protein composed of VEGFR1 domain 2 and VEGFR2 domain 3, which bind to and neutralize VEGF-A, VEGF-B, and PlGF.[33,34] VEGF-trap has been approved by the Food and Drug Administration for use in patients with colorectal cancer or age-related macular degeneration.[34,35] PB101 is a glycosylated soluble decoy receptor fusion protein composed of VEGFR1 domains 2 and 3, and also captures VEGF-A, VEGF-B, and PlGF.[27,29] Both VEGF-trap and PB101 have been reported to bind to PlGF; however, PB101 binds to PlGF more strongly than to VEGF-trap because of differences in protein structure.[27] Therefore, we investigated whether this difference could affect the mechanisms of action of drugs within tumors, especially on tumor immunity. We treated MC38 tumor-bearing mice with control, VEGF-trap, or PB101 (Figure 4a). Although PB101 and VEGF-trap did not differ in terms of tumor growth suppression (Figure 4b), they showed distinct patterns of immune reprogramming within the tumors. Compared with the VEGF trap, PB101 markedly activated innate immunity by increasing the number of $CD11c^+$ dendritic cells (Figure 4c). Additionally, PB101 and VEGF-trap similarly reduced the numbers of M2-like TAMs; however, PB101 increased the number of M1-like macrophages compared to VEGF-trap, thereby increasing the M1/M2 ratio (Figure 4d). Notably, PB101 markedly increased the number of $GzmB^+$-activated $CD8^+$ T cells and slightly increased the number of $FoxP3^+CD4^+$ regulatory T cells, whereas VEGF-trap did not increase the number of activated $CD8^+$ T cells, but markedly increased that of regulatory T cells (Figure 4e). Therefore, the ratio of $CD8^+$ T cells to regulatory T cells was higher in PB101-treated tumors than in VEGF-trap-treated tumors. NanoString Immune Profiling revealed consistent results for innate and adaptive immune activation (Figure 4g). Key activators of innate immunity, such as *Mavs*, *Sting* (*Tmem173*), and *Myd88*, were more strongly upregulated in tumors treated with PB101 than in those treated with VEGF-trap (Figure 4h). Moreover, the cytotoxic lymphocyte gene *Gzma* was upregulated in PB101-treated tumors (Figure 4i). Although tumoral *Vegfa* and *Plgf* was highly induced after VEGF-trap treatment, *Vegfa* was not induced and *Plgf* was downregulated after PB101 treatment. VEGF-A is transcriptionally regulated by hypoxia-inducible factor-1 (HIF-1), and PlGF is regulated by cAMP response element binding protein (CREB).[36–38] Notably, VEGF-trap substantially induced *Hif1a* and *Creb* expression compared to the control, whereas PB101 did not. Overall, PB101 could elicit more potent innate and adaptive immunity in tumors than VEGF-trap.

Combination immunotherapy of PB101 and anti-PD-L1 further suppressed tumor progression and prolonged overall survival

Although PB101 monotherapy elicited considerable antitumor immunity, its efficacy was not sufficient to induce complete tumor regression. Because PD-1/PD-L1 axis is important target for cancer immunotherapy and PD-1 was upregulated following PB101 treatment (Figure 3b), we investigated whether the combined blockade of PD-L1 could further enhance the antitumor efficacy of PB101 (Figure 5a). While PB101 or anti-PD-L1 monotherapy showed comparable tumor growth suppression, the combination therapy induced stronger suppression of MC38 tumor growth (Figure 5b).

To further validate these results, we evaluated the efficacy of combination therapy in a murine liver cancer model (Hepa-V) (Figure 5c). Although PB101 monotherapy was comparable to anti-PD-L1 monotherapy in terms of tumor control and survival outcomes, the combination therapy of PB101 and anti-PD-L1 showed the strongest tumor growth suppression and longest overall survival (Figure 5d,e). Notably, three mice in the combination group showed complete tumor regression and remained tumor-free for over 90 days (Figure 5e). Overall, PB101 synergized with anti-PD-L1 to suppress tumor growth and prolong overall survival.

Combination immunotherapy of PB101 and anti-PD-L1 provide long-term immune protection against recurrence and hematogenous lung metastasis

To confirm long-term immune memory, mice that experienced complete liver cancer regression after PB101 and anti-PD-L1 combination therapy were subcutaneously and intravenously re-challenged with liver cancer cells on day 91 (Figure 6a). We observed that mice that experienced complete tumor regression after combination immunotherapy were completely immune to liver cancer recurrence and remained tumor-free compared to control mice (Figure 6b). Moreover, these mice showed significantly suppressed hematogenous lung metastasis compared to the control mice (Figure 6c,d). Therefore, PB101 and anti-PD-L1 combination therapy can induce long-lasting antitumor immune memory against recurrence and metastasis, thereby prolonging overall survival.

Discussion

In this study, we demonstrated that PB101 exerts antitumor effects through robust immune reprogramming as well as previously known antiangiogenic mechanisms. PB101 enhanced dendritic cell activity and promoted macrophage polarization toward M1 within tumors. Moreover, PB101 facilitated the infiltration of GzB^+-activated $CD8^+$ T cells into tumors. As the antitumor effect of PB101 in immunocompetent tumor models was substantially reduced in the absence of IFN-γ and $CD8^+$ T cells, the mode of action of PB101 appears to be more dependent on tumor immune reprogramming than on anti-angiogenesis.

The mechanisms of action of PB101 are distinct from those of VEGF-trap (aflibercept), a previously developed decoy receptor used in clinical practice. First, PB101 enhanced antitumor innate immunity more strongly than VEGF-trap. Second, regarding adaptive immunity, PB101 increased the number of $CD8^+$ T cells to a greater extent than that of T_{reg} leading to a high $CD8^+/T_{reg}$ ratio; however, VEGF-trap increased the number of T_{regs} to a greater extent than that of $CD8^+$, thus lowering the $CD8^+/T_{reg}$ ratio. Therefore, PB101

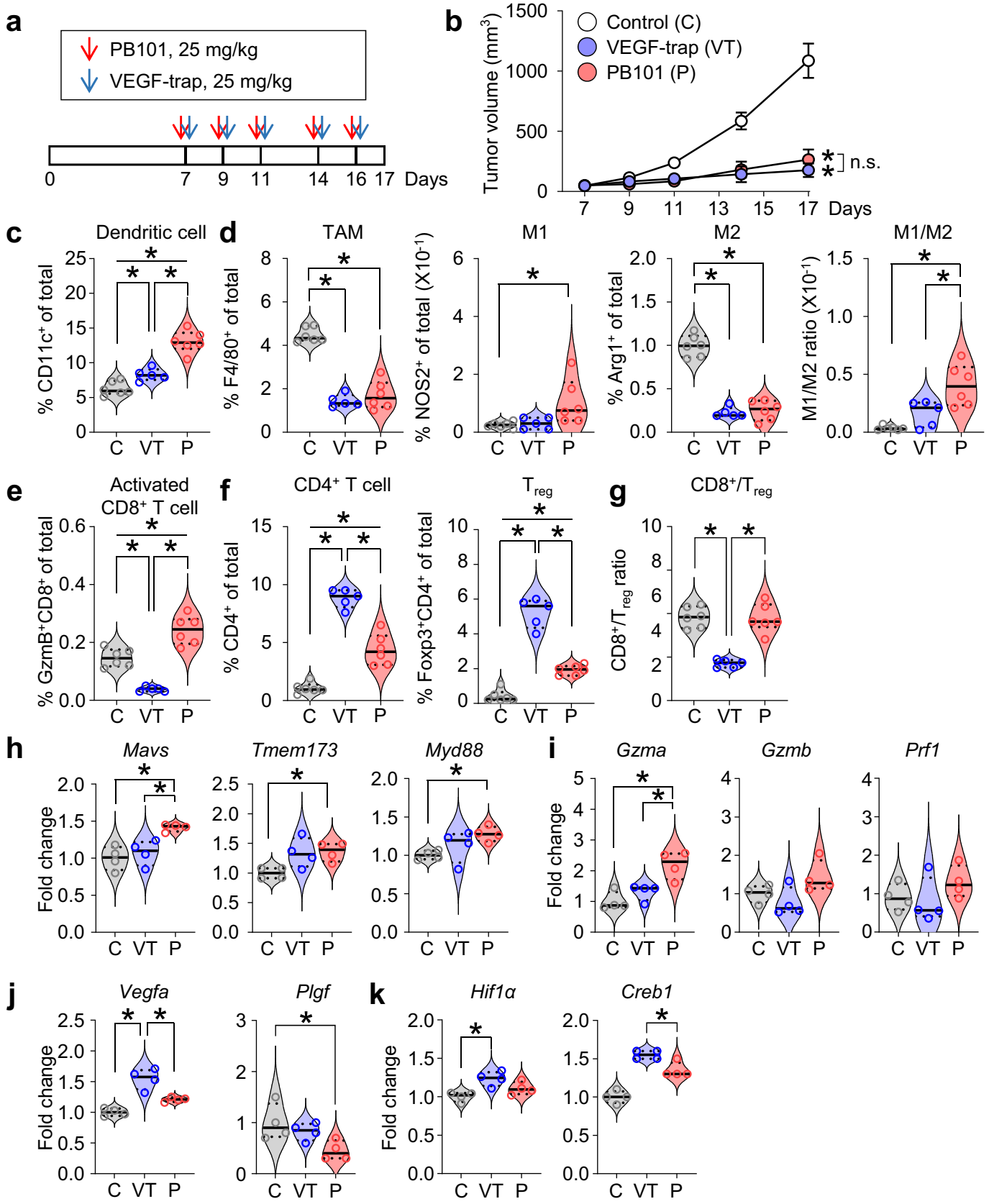

Figure 4. PB101 shows distinct immunologic mechanisms of action compared to VEGF-trap. a. Diagram depicting treatment schedule. b. Comparison of MC38 tumor growth. C – G. Comparisons of dendritic cell (c), TAMs, M1/M2-like macrophages, M1/M2 ratio (d), activated $CD8^+$ T cell (e), $CD4^+$ T cell, regulatory T cell (T_{reg}) (f), and $CD8^+$ T cell ($CD8^+$) and T_{reg} ratio within the tumor (g). H – K. Comparisons of gene expressions related to innate immunity (*mavs, Tmem173, and Myd88*) (h), cytotoxic lymphocytes (*Gzma*, *Gzmb*, *Prf1*) (i), angiogenesis (*Vegfa, Plgf*) (j), and transcription factors (*Hif1α* and *Creb1*) (k). Values are shown as the mean ± SD. *$P < .05$.

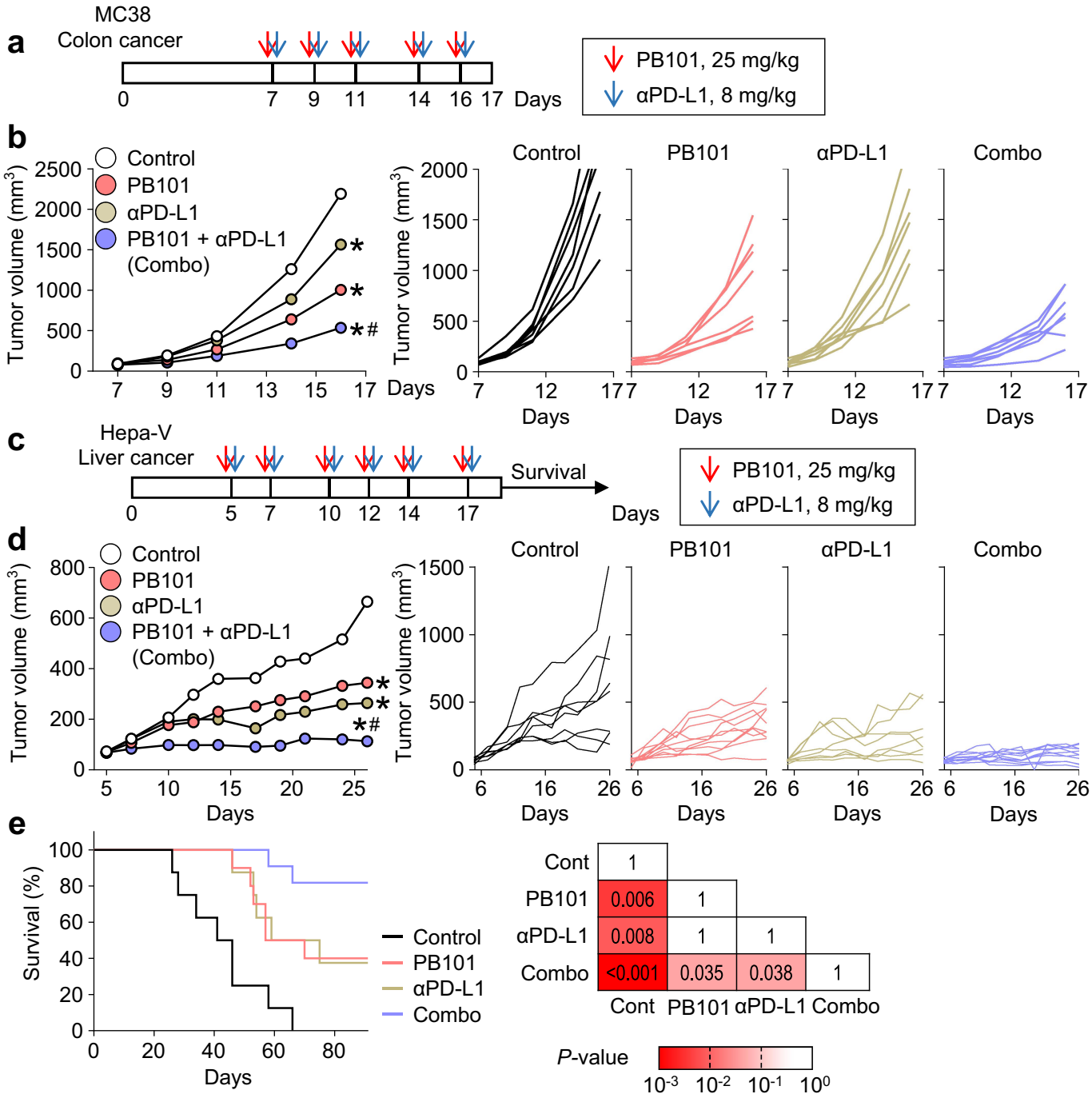

Figure 5. Combination immunotherapy of PB101 and anti-PD-L1 further suppressed tumor progression and prolonged overall survival. a. Diagram depicting treatment schedule in MC38 colon cancer. b. Comparison of MC38 colon cancer growth. Mean and individual tumor growth curves over time. N = 7 per group. c. Diagram depicting treatment schedule in Hepa-V liver cancer. d. Comparison of liver cancer growth. Mean and individual tumor growth curves over time e. Kaplan-Meier survival curves showing overall survival of liver cancer-bearing mice. Table shows P-values determined by log-rank test. Values are shown as the mean ± SD. *$P < .05$ vs. control, *$P < .05$ vs. PB101. N = 8–11 per group.

may be more effective than VEGF-trap in T-cell-targeted cancer immunotherapy. Another point of distinction is the regulation of VEGF-A and PlGF, the molecular targets of PB101 and VEGF-trap. VEGF-trap induced strong rebound transcription of VEGF-A, whereas PB101 did not. Moreover, VEGF-trap did not affect PlGF expression, whereas PB101 reduced PlGF transcription. This difference may be attributed to the fact that HIF1A and CREB1, which are important transcription factors for VEGF-A and PlGF, respectively, are highly induced in tumors treated with VEGF-trap but not with PB101.

Until the mid-2010s, the clinical development of antiangiogenic agents focused on demonstrating potent antiangiogenic effects and strong tumor growth inhibition.[3] Recently, however, major clinical advances in the combination treatment of liver and kidney cancers using antiangiogenic agents and immune checkpoint inhibitors have provided a new perspective on the optimal roles of antiangiogenic agents in cancer therapy.[3,12–14] In clinical trials, antiangiogenic agents have shown stronger and longer-lasting therapeutic efficacy when used as components of cancer immunotherapy than when used as a monotherapy or used in

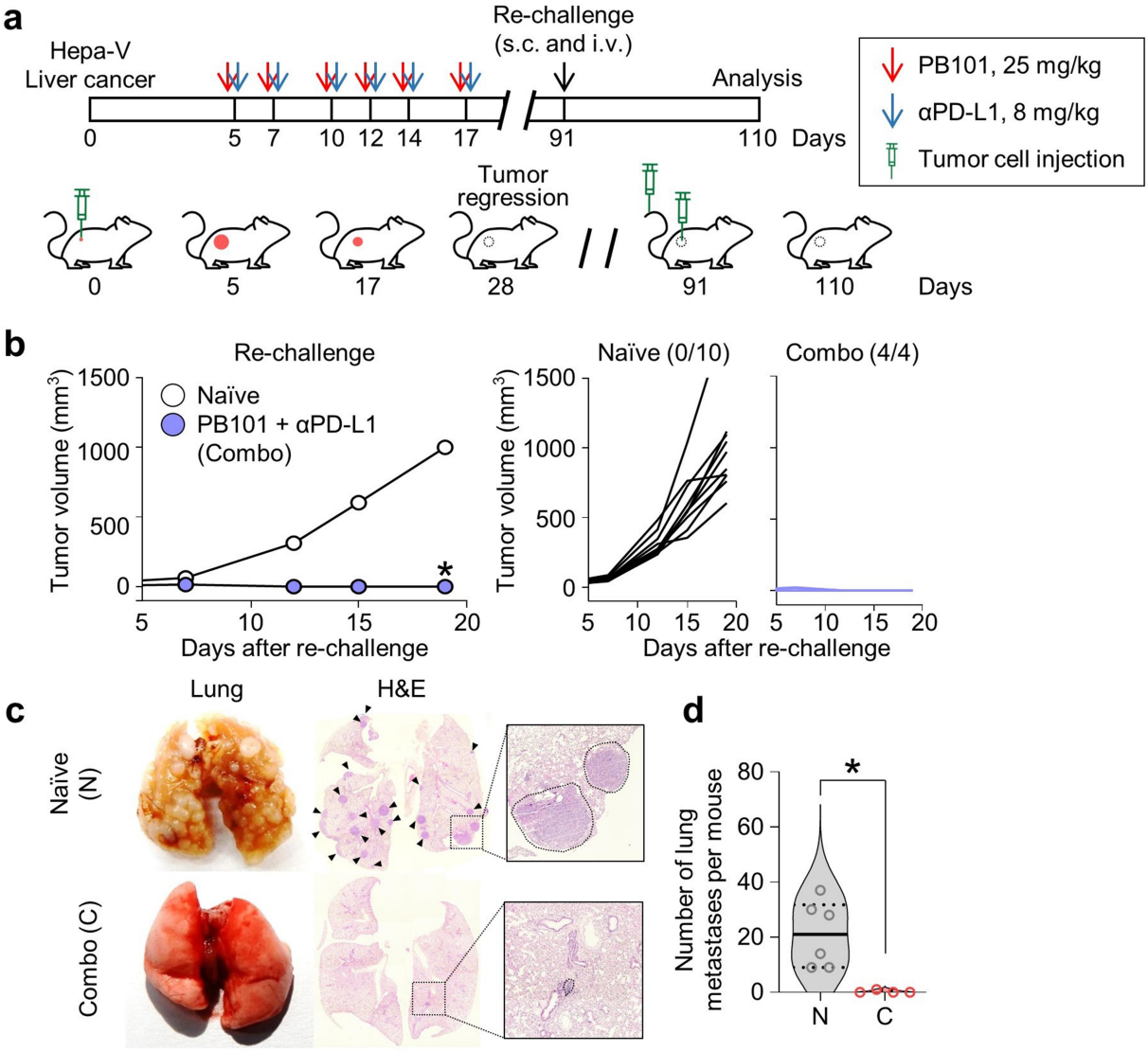

Figure 6. Combination immunotherapy of PB101 and anti-PD-L1 provide long-term immune protection against recurrence and metastasis. a. Diagram depicting re-challenge schedule in Hepa-V liver cancer. Red and blue arrows indicate treatments and black arrow indicates subcutaneous and intravenous re-challenge of Hepa-V liver cancer cells. b. Comparison of Hepa-V tumor growth. Mean and individual tumor growth curves over time. N = 4–10 per group. c. Representative gross images and hematoxylin and eosin (H&E) staining images of lung. Arrow heads indicate pulmonary metastatic lesions. d. Comparison of the number of metastatic colonies per lung section. Values are shown as mean ± SD. *P < .05 vs naïve. N = 4–6 per group.

combination with cytotoxic chemotherapy.[3,12,13,15] Therefore, future antiangiogenic drug development must be pursued in the context of cancer immunotherapy. However, not all antiangiogenic agents are immunologically equivalent when combined with immune checkpoint inhibitors. For example, lenvatinib, cabozantinib, and axitinib successfully synergized with immune checkpoint inhibitors in renal cell carcinoma, whereas pazopanib and sunitinib did not.[13,14,39,40] This may be because different antiangiogenic drugs have different levels of antitumor immune reprogramming apart from their antiangiogenic capabilities. Therefore, to develop successful combination immunotherapy, the immunological ability of each drug should be fully evaluated and understood. In this regard, PB101 has the potential to be used in combination therapy with immune checkpoint inhibitors in the future.

Scheduling combination therapy with antiangiogenic drugs and anti-PD-L1 inhibitors may affect therapeutic outcomes. Previous preclinical studies showed that antiangiogenic therapy prior to anti-PD-L1 therapy may prime the TME to be more susceptible to anti-PD-L1 treatment, thus having superior efficacy compared to simultaneous therapy.[41,42] One in silico study using a mathematical simulation showed that sequential treatment with anti-VEGF therapy followed by anti-PD-1 therapy could have stronger antitumor effects than simultaneous treatment.[43] However, this hypothesis has not yet been demonstrated in patients with cancer. In clinical setting, treatment is repeated every 2 or 3 weeks as long as the cancer does not progress and toxicities are tolerable; thus, the distinction between sequential and simultaneous treatment is ambiguous. Therefore, all currently approved combinations of antiangiogenic therapy and immune checkpoint inhibitors are administered simultaneously to patients with cancer. Therefore, in the present study, we attempted to simultaneously administer PB101 and anti-PD-L1. However, it is important to confirm whether the different schedules have different therapeutic and immunomodulatory effects in future studies.

In this study, we investigated the effect of PB101 on tumor immunity, but several questions still remain. First, we focused on the interaction between PB101 and VEGFR1, a common receptor for both VEGF-A and PlGF. However, PB101 also binds to VEGF-B with a low affinity, which is comparable to VEGF-trap.[27] Therefore, we cannot exclude the involvement of VEGF-B in PB101-mediated tumor immune modulation. Moreover, because VEGF-A can bind to and activate VEGFR1 and VEGFR2 in tumor endothelial cells,[44] PB101 binding to VEGF-A may affect VEGFR2 signaling and the VEGFR2-mediated regulation of tumor angiogenesis. Second, the ectopic tumor models employed in the present study provide rapid tumor growth, easy monitoring and measurement, and a controlled tumor microenvironment. However, orthotopic or immunoreconstituted PDX models may provide more clinically relevant insights into the PB101-induced remodeling of the tumor immune microenvironment than ectopic models. Third, as individualized cancer therapy has gained considerable attention, the influence of sex has become increasingly crucial. Specifically, the menstrual cycles of females may affect the levels of sex hormones, such as estrogen or progesterone, which can affect neovessel formation during tumor progression. The major targets of PB101, VEGF-A, and PlGF could be affected and regulated by sex hormones. VEGF-A is regulated by progesterone and itself regulates vascular remodeling.[45] Moreover, PlGF is a placenta-derived angiogenic factor and its expression is sensitive to sex hormones.[46] Therefore, it is plausible that changes in female sex hormones during the menstrual cycle may affect VEGF and PlGF expression and thus influence the antitumor effects of PB101 in tumor-bearing female animals.

In conclusion, PB101 inhibits tumor progression through the robust activation of antitumor immunity, which is distinct from VEGF-trap. Combination therapy with PB101 and anti-PD-L1 can eradicate tumor cells and establish durable protective immunity against tumor recurrence and metastasis. These findings provide the scientific rationales for further clinical development of PB101 in advanced cancers.

Disclosure statement

CK and HJC has received research grants from Panolos Bioscience. HGY, JAS, and HSL are full-time employees of Panolos Bioscience. The other authors have no potential conflicts of interest to disclose.

Funding

This work was supported by the National Research Foundation of Korea [NRF] grants funded by the Korean government [MSIT] [NRF-2023R1A2C2006375 to CK and NRF-2023R1A2C2004339 to HJC]. This work was supported by Panolos Bioscience, Inc.

ORCID

Hannah Yang http://orcid.org/0000-0003-2252-7041
Hong Jae Chon http://orcid.org/0000-0002-6979-5812
Chan Kim http://orcid.org/0000-0001-9780-6155

Author contributions

Study concept and design: EJG, HY, HGY, HSL, HJC, CK. Data curation and formal analysis: EJG, HY, SJL, WSL, HJC, CK. Investigation and data interpretation: All authors. Manuscript preparation: EJG, HY, SJL, HJC, CK. Approved the final manuscript: All authors.

Availability of data and materials

The dataset analyzed during the current study is available from the corresponding author on reasonable request.

Ethics approval

All mouse experiments were approved by the Institutional Animal Care and Use Committee (IACUC, #230015) of CHA University.

References

1. Kerbel RS. Tumor angiogenesis. N Engl J Med. 2008;358(19):2039–2049. doi:10.1056/NEJMra0706596.
2. Augustin HG, Koh GY. Antiangiogenesis: vessel regression, vessel normalization, or both? Cancer Res. 2022;82(1):15–17. doi:10.1158/0008-5472.CAN-21-3515.
3. Lee WS, Yang H, Chon HJ, Kim C. Combination of anti-angiogenic therapy and immune checkpoint blockade normalizes vascular-immune crosstalk to potentiate cancer immunity. Exp Mol Med. 2020;52(9):1475–1485. doi:10.1038/s12276-020-00500-y.
4. Fukumura D, Kloepper J, Amoozgar Z, Duda DG, Jain RK. Enhancing cancer immunotherapy using antiangiogenics: opportunities and challenges. Nat Rev Clin Oncol. 2018;15(5):325–340. doi:10.1038/nrclinonc.2018.29.
5. Kim C, Yang H, Fukushima Y, Saw P, Lee J, Park J-S, Park I, Jung J, Kataoka H, Lee D, et al. Vascular RhoJ is an effective and selective target for tumor angiogenesis and vascular disruption. Cancer Cell. 2014;25(1):102–117. doi:10.1016/j.ccr.2013.12.010.
6. Park J-S, Kim I-K, Han S, Park I, Kim C, Bae J, Oh SJ, Lee S, Kim JH, Woo D-C, et al. Normalization of tumor vessels by Tie2 activation and Ang2 inhibition enhances drug delivery and produces a favorable tumor microenvironment. Cancer Cell. 2016;30(6):953–967. doi:10.1016/j.ccell.2016.10.018.
7. Ebos JM, Lee CR, Cruz-Munoz W, Bjarnason GA, Christensen JG, Kerbel RS. Accelerated metastasis after short-term treatment with a potent inhibitor of tumor angiogenesis. Cancer Cell. 2009;15(3):232–239. doi:10.1016/j.ccr.2009.01.021.
8. Paez-Ribes M, Allen E, Hudock J, Takeda T, Okuyama H, Viñals F, Inoue M, Bergers G, Hanahan D, Casanovas O, et al. Antiangiogenic therapy elicits malignant progression of tumors to increased local invasion and distant metastasis. Cancer Cell. 2009;15(3):220–231. doi:10.1016/j.ccr.2009.01.027.
9. Kim CW, Chon HJ, Kim C. Combination immunotherapies to overcome intrinsic resistance to checkpoint blockade in microsatellite stable colorectal cancer. Cancers. 2021;13(19):4906. doi:10.3390/cancers13194906.
10. Aguiar R, Moraes J. Exploring the immunological mechanisms underlying the anti-vascular endothelial growth factor activity in tumors. Front Immunol. 2019;10:1023. doi:10.3389/fimmu.2019.01023.
11. Khan KA, Kerbel RS. Improving immunotherapy outcomes with anti-angiogenic treatments and vice versa. Nat Rev Clin Oncol. 2018;15(5):310–324. doi:10.1038/nrclinonc.2018.9.
12. Finn RS, Qin S, Ikeda M, Galle PR, Ducreux M, Kim T-Y, Kudo M, Breder V, Merle P, Kaseb AO, et al. Atezolizumab plus bevacizumab in unresectable hepatocellular carcinoma. N Engl J Med. 2020;382(20):1894–1905. doi:10.1056/NEJMoa1915745.
13. Motzer R, Alekseev B, Rha S-Y, Porta C, Eto M, Powles T, Grünwald V, Hutson TE, Kopyltsov E, Méndez-Vidal MJ, et al. Lenvatinib plus pembrolizumab or everolimus for advanced renal cell carcinoma. N Engl J Med. 2021;384(14):1289–1300. doi:10.1056/NEJMoa2035716.
14. Rini BI, Plimack ER, Stus V, Gafanov R, Hawkins R, Nosov D, Pouliot F, Alekseev B, Soulières D, Melichar B, et al. Pembrolizumab plus axitinib versus sunitinib for advanced

renal-cell carcinoma. N Engl J Med. 2019;380(12):1116–1127. doi:10.1056/NEJMoa1816714.
15. Socinski MA, Jotte RM, Cappuzzo F, Orlandi F, Stroyakovskiy D, Nogami N, Rodríguez-Abreu D, Moro-Sibilot D, Thomas CA, Barlesi F, et al. Atezolizumab for first-line treatment of metastatic nonsquamous NSCLC. N Engl J Med. 2018;378(24):2288–2301. doi:10.1056/NEJMoa1716948.
16. Makker V, Colombo N, Casado Herráez A, Santin AD, Colomba E, Miller DS, Fujiwara K, Pignata S, Baron-Hay S, Ray-Coquard I, et al. Lenvatinib plus pembrolizumab for advanced endometrial cancer. N Engl J Med. 2022;386(5):437–448. doi:10.1056/NEJMoa2108330.
17. Ribatti D. The discovery of the placental growth factor and its role in angiogenesis: a historical review. Angiogenesis. 2008;11 (3):215–221. doi:10.1007/s10456-008-9114-4.
18. Albonici L, Giganti MG, Modesti A, Manzari V, Bei R. Multifaceted role of the placental growth factor (PlGF) in the antitumor immune response and cancer progression. Int J Mol Sci. 2019;20(12):2970. doi:10.3390/ijms20122970.
19. Selvaraj SK, Giri RK, Perelman N, Johnson C, Malik P, Kalra VK. Mechanism of monocyte activation and expression of proinflammatory cytochemokines by placenta growth factor. Blood. 2003;102(4):1515–1524. doi:10.1182/blood-2002-11-3423.
20. Cao Y. Positive and negative modulation of angiogenesis by VEGFR1 ligands. Sci Signal. 2009;2(59):re1–re1. doi:10.1126/scisignal.259re1.
21. Zhou Y, Tu C, Zhao Y, Liu H, Zhang S. Placental growth factor enhances angiogenesis in human intestinal microvascular endothelial cells via PI3K/Akt pathway: potential implications of inflammation bowel disease. Biochem Bioph Res Co. 2016;470 (4):967–974. doi:10.1016/j.bbrc.2016.01.073.
22. Snuderl M, Batista A, Kirkpatrick ND, Ruiz de Almodovar C, Riedemann L, Walsh E, Anolik R, Huang Y, Martin J, Kamoun W, et al. Targeting placental growth factor/neuropilin 1 pathway inhibits growth and spread of medulloblastoma. Cell. 2013;152(5):1065–1076. doi:10.1016/j.cell.2013.01.036.
23. He C, Zhu K, Bai X, Li Y, Sun D, Lang Y, Ning J, Sun F, Qu C, Xu S, et al. Placental growth factor mediates crosstalk between lung cancer cells and tumor-associated macrophages in controlling cancer vascularization and growth. Cell Physiol Biochem. 2018;47 (6):2534–2543. doi:10.1159/000491650.
24. Voron T, Colussi O, Marcheteau E, Pernot S, Nizard M, Pointet A-L, Latreche S, Bergaya S, Benhamouda N, Tanchot C, et al. VEGF-A modulates expression of inhibitory checkpoints on CD8+ T cells in tumors. J Exp Med. 2015;212(2):139–148. doi:10.1084/jem.20140559.
25. Kim CG, Jang M, Kim Y, Leem G, Kim KH, Lee H, Kim T-S, Choi SJ, Kim H-D, Han JW, et al. VEGF-A drives TOX-dependent T cell exhaustion in anti–PD-1–resistant microsatellite stable colorectal cancers. Sci Immunol. 2019;4(41):eaay0555. doi:10.1126/sciimmunol.aay0555.
26. Shin J-Y, Yoon I-H, Kim J-S, Kim B, Park C-G. Vascular endothelial growth factor-induced chemotaxis and IL-10 from T cells. Cell Immunol. 2009;256(1–2):72–78. doi:10.1016/j.cellimm.2009.01.006.
27. Lee J-E, Kim C, Yang H, Park I, Oh N, Hua S, Jeong H, An HJ, Kim SC, Lee GM, et al. Novel glycosylated VEGF decoy receptor fusion protein, VEGF-Grab, efficiently suppresses tumor angiogenesis and ProgressionStructure-based design of novel antiangiogenic biologics. Mol Cancer Ther. 2015;14(2):470–479. doi:10.1158/1535-7163.MCT-14-0968-T.
28. Hong HK, Park YJ, Kim DK, Ryoo N-K, Ko Y-J, Park KH, Kim HM, Woo SJ. Preclinical efficacy and safety of VEGF-grab, a novel anti-VEGF drug, and its comparison to aflibercept. Invest Ophthalmol Visual Sci. 2020;61(13):22–22. doi:10.1167/iovs.61.13.22.
29. Park I, Yang H, Park J-S, Koh GY, Choi EK. VEGF-Grab enhances the efficacy of radiation therapy by blocking VEGF-A and treatment-induced PlGF. Int J Radiat Oncol. 2018;102 (3):609–618. doi:10.1016/j.ijrobp.2018.06.401.
30. Yang H, Lee WS, Kong SJ, Kim CG, Kim JH, Chang SK, Kim S, Kim G, Chon HJ, Kim C, et al. STING activation reprograms tumor vasculatures and synergizes with VEGFR2 blockade. J Clin Invest. 2019;129(10):4350–4364. doi:10.1172/JCI125413.
31. Lee SJ, Yang H, Kim WR, Lee YS, Lee WS, Kong SJ, Lee HJ, Kim JH, Cheon J, Kang B, et al. STING activation normalizes the intraperitoneal vascular-immune microenvironment and suppresses peritoneal carcinomatosis of colon cancer. J Immunother Cancer. 2021;9(6):e002195. doi:10.1136/jitc-2020-002195.
32. Park HS, Kim YM, Kim S, Lee WS, Kong SJ, Yang H, Kang B, Cheon J, Shin S-J, Kim C, et al. High endothelial venule is a surrogate biomarker for T-cell inflamed tumor microenvironment and prognosis in gastric cancer. J Immunother Cancer. 2021;9(10):e003353. doi:10.1136/jitc-2021-003353.
33. Holash J, Davis S, Papadopoulos N, Croll SD, Ho L, Russell M, Boland P, Leidich R, Hylton D, Burova E, et al. VEGF-Trap: a VEGF blocker with potent antitumor effects. Proc Natl Acad Sci USA. 2002;99(17):11393–11398. doi:10.1073/pnas.172398299.
34. Ciombor KK, Berlin J. Aflibercept—a decoy VEGF receptor. Curr Oncol Rep. 2014;16(2):1–7. doi:10.1007/s11912-013-0368-7.
35. Heier JS, Brown DM, Chong V, Korobelnik J-F, Kaiser PK, Nguyen QD, Kirchhof B, Ho A, Ogura Y, Yancopoulos GD, et al. Intravitreal aflibercept (VEGF trap-eye) in wet age-related macular degeneration. Ophthalmology. 2012;119(12):2537–2548. doi:10.1016/j.ophtha.2012.09.006.
36. Kim Y, Nam HJ, Lee J, Park DY, Kim C, Yu YS, Kim D, Park SW, Bhin J, Hwang D, et al. Methylation-dependent regulation of HIF-1α stability restricts retinal and tumour angiogenesis. Nat Commun. 2016;7(1):10347. doi:10.1038/ncomms10347.
37. Maxwell PH, Wiesener MS, Chang G-W, Clifford SC, Vaux EC, Cockman ME, Wykoff CC, Pugh CW, Maher ER, Ratcliffe PJ, et al. The tumour suppressor protein VHL targets hypoxia-inducible factors for oxygen-dependent proteolysis. Nature. 1999;399 (6733):271–275. doi:10.1038/20459.
38. Depoix C, Tee MK, Taylor RN. Molecular regulation of human placental growth factor (PlGF) gene expression in placental villi and trophoblast cells is mediated via the protein kinase a pathway. Reprod Sci. 2011;18(3):219–228. doi:10.1177/1933719110389337.
39. Choueiri TK, Powles T, Burotto M, Escudier B, Bourlon MT, Zurawski B, Oyervides Juárez VM, Hsieh JJ, Basso U, Shah AY, et al. Nivolumab plus cabozantinib versus sunitinib for advanced renal-cell carcinoma. N Engl J Med. 2021;384(9):829–841. doi:10.1056/NEJMoa2026982.
40. Amin A, Plimack ER, Ernstoff MS, Lewis LD, Bauer TM, McDermott DF, Carducci M, Kollmannsberger C, Rini BI, Heng DYC, et al. Safety and efficacy of nivolumab in combination with sunitinib or pazopanib in advanced or metastatic renal cell carcinoma: the CheckMate 016 study. J Immunotherapy Cancer. 2018;6(1):1–12. doi:10.1186/s40425-018-0420-0.
41. Allen E, Jabouille A, Rivera LB, Lodewijckx I, Missiaen R, Steri V, Feyen K, Tawney J, Hanahan D, Michael IP, et al. Combined antiangiogenic and anti–PD-L1 therapy stimulates tumor immunity through HEV formation. *science translational medicine*. Sci Transl Med. 2017;9(385):eaak9679. doi:10.1126/scitranslmed.aak9679.
42. Schmittnaegel M, Rigamonti N, Kadioglu E, Cassará A, Wyser Rmili C, Kiialainen A, Kienast Y, Mueller H-J, Ooi C-H, Laoui D, et al. Dual angiopoietin-2 and VEGFA inhibition elicits antitumor immunity that is enhanced by PD-1 checkpoint blockade. Sci Transl Med. 2017;9(385):eaak9670. doi:10.1126/scitranslmed.aak9670.
43. Lai X, Friedman A. How to schedule VEGF and PD-1 inhibitors in combination cancer therapy? BMC Syst Biol. 2019;13(1):1–18. doi:10.1186/s12918-019-0706-y.
44. Shibuya M. Differential roles of vascular endothelial growth factor receptor-1 and receptor-2 in angiogenesis. BMB Rep. 2006;39 (5):469–478. doi:10.5483/BMBRep.2006.39.5.469.
45. Kim M, Park HJ, Seol JW, Jang JY, Cho Y-S, Kim KR, Choi Y, Lydon JP, DeMayo FJ, Shibuya M, et al. VEGF - A regulated by progesterone governs uterine angiogenesis and vascular remodelling during pregnancy. EMBO Mol Med. 2013;5(9):1415–1430. doi:10.1002/emmm.201302618.
46. Donnini S, Machein MR, Plate KH, Weich HA. Expression and localization of placenta growth factor and PlGF receptors in human meningiomas. J Pathol. 1999;189(1):66–71. doi:10.1002/(SICI)1096-9896(199909)189:1<66:AID-PATH390>3.0.CO;2-X.